Coarsening and Morphology of β' Particles in Fe-Ni-Al-Mo Ferritic Alloys

H. A. CALDERON, M. E. FINE, and J. R. WEERTMAN

Studies have been carried out of the effect of aging at 973 K on the ordered NiAl β' precipitate particles in a series of Fe-Ni-Al alloys with and without the addition of Mo. The lattice parameter disregistry between matrix and precipitates is affected by the Mo content. The rate of precipitate coarsening during isothermal aging is slowest when the misfit is minimized. The dependence of coarsening upon misfit is more pronounced in alloys with low precipitate volume fractions. Raising the precipitate volume fraction increases β' coarsening rates more than predicted by theory. The lattice parameters of both the β' particles and the matrix are functions of aging time. Compositional changes, segregation of Mo to the particle-matrix interface and, at long aging times, loss of coherency are proposed as causes of the observed lattice parameter changes. The addition of Mo to the Fe-Ni-Al alloys causes the β' particles to remain spherical even after extended periods of aging whereas the particles become somewhat cubic or rectangular parallelepiped in form in the Mo-free alloys. The size distributions of the β' particles agree in a general way with the predictions of the Brailsford and Wynblatt and Voorhees and Glicksman models, but are somewhat less skewed and do not show the predicted sharp cutoff in particle size on the high radius side.

I. INTRODUCTION

MODERN Ni-base superalloys depend upon the presence of γ' ($L1_2$ structure) precipitates for their excellent mechanical properties at elevated temperature. These precipitates are coherent and coplanar with the matrix as well as thermodynamically stable. These crystallographic characteristics lead to strengthening by mechanisms such as the creation of antiphase boundaries or coherency strains that effectively impede dislocation motion. By analogy, a successful iron base alloy for high temperature application might be expected to make use of second phase particles with similar properties. β' (NiAl-type) precipitates which have a B2 (CsCl) structure satisfy this requirement in bcc ferritic alloys. The reported lattice parameter of β' is 0.2887 nm and that of ferrite is 0.2866 nm.[1] The most common commercial Fe-base alloys which make use of NiAl-type particles for precipitation hardening purposes are 17-7 PH steel (17Cr-7Ni-1.2Al-0.07C, wt pct) and Nitralloy-N steel (0.2C-4.8Ni-1.9Al-0.5Cr-0.4Mn-0.2Mo, wt pct). These alloys are ferritic only at relatively low temperatures. Their low α to γ transformation temperature impedes their use at an elevated temperature.

The Fe-Ni-Al system has been investigated by Bradley[2] and Kolesar.[3] The latter paid attention to the Fe-rich portion of the system. Analysis of the ternary diagram shows that if sufficient Al is present, ferritic Fe-base alloys containing NiAl type precipitates may be obtained over a wide range of compositions and volume fractions.

The present investigation concerns Fe-Ni-Al-Mo alloys containing β' particles. Molybdenum was added in minor amounts to vary the lattice mismatch between β' and the ferritic matrix. The effect of mismatch on Ostwald ripening of the β' particles was determined.

As suggested by one of the authors,[4] control of the interfacial energy in the semi-coherent regime may be possible by manipulation of the lattice parameter disregistry δ between matrix and precipitate. In turn, the value of δ is expected to affect the rate of Ostwald ripening. In an earlier report,[5] the kinetics of coarsening of β' in two alloys with different lattice mismatches were described. However, the influence of δ on coarsening was clouded by the use of different precipitate volume fractions and global compositions. The present investigation was planned to assess conclusively the effect of δ by means of controlled additions of Mo to otherwise identical alloys.

Several theoretical models have been proposed to describe volume diffusion controlled Ostwald ripening of precipitates in fluid matrices.[6–10] These models predict that the volume fraction of precipitate will affect the coarsening process of second phase particles. The present investigation has as one of its main objectives the experimental analysis of the effect of precipitate volume fraction on Ostwald ripening. This subject was preliminarily addressed in a previous publication.[11] Additional analysis is given in the present report.

No theoretical models have been developed to describe the Ostwald ripening of an ensemble of solid precipitates in a solid matrix. The complications of elastic interactions, changes of molar volume of solute on crossing the particle-matrix interface, applied stresses, and the need for redefining well-known thermodynamic quantities, *e.g.*, chemical potentials, all make the study of coarsening in solid matrices very difficult. A complete theoretical solution is lacking at present. The advances made by Larché and Cahn[12] and by Voorhees and Johnson[13,14] are noteworthy and a comprehensive model for the coarsening of solid particles in solid matrices may be available in the near future. Nevertheless, experiments on solid alloys with perfectly fitting coherent precipitates may allow comparison with the theoretical models developed for fluids since the effects of elastic strain energy on the coarsening process are reduced. In addition,

H. A. CALDERON is Postdoctoral Fellow, Swiss Federal Institute of Technology, Zurich, ETH-Honggerberg, CH-8093, Zurich, Switzerland. M. E. FINE, Walter P. Murphy Professor, and J. R. WEERTMAN, Professor and Chairman, are with the Department of Materials Science and Engineering, Northwestern University, 2145 Sheridan Road, Evanston, IL 60208.

Manuscript submitted July 10, 1987.

the effects of strain energy may be inferred by reference to the results obtained in the case of misfitting particles.

The detailed analysis of solids made by Cahn and Larché[15] has shown that surface stresses influence the interfacial energy. It is necessary to include the effect of surface stresses in order to describe correctly a solid-solid interface. It is commonly believed that the morphology of a coherent particle depends upon the lattice parameter mismatch with the matrix. (This constrained misfit, as correctly pointed out by Nathal,[16] cannot be measured in extracted particles or pure intermetallics without consideration of the fact that the particles embedded in solid alloys are elastically constrained.) However, on the basis of Cahn and Larché's treatment it is possible to conclude that the morphology of a coherent particle in a solid system depends not only on the lattice parameter misfit but also on achievement of chemical equilibrium at the interface. There has been little experimental work in this area despite the pioneering research of Havalda *et al.*,[17] who showed that the morphology of incoherent γ' in Ni alloys depends on the interfacial surface stress rather than only on the unconstrained lattice misfit. In the present report experimental observations on the effect of Mo on particle morphology are described.

To summarize, in this study of coherent or semi-coherent β' particles in a ferritic iron alloy, research was performed in order to:

1. examine the effect of δ on the rate of particle coarsening in a series of alloys in which the particle volume fraction f_v is kept constant;
2. measure the influence of f_v on coarsening rates, and compare the results with theoretical predictions;
3. observe particle morphology in the presence of Mo.

II. EXPERIMENTAL PROCEDURES

Some of the alloys used for this study were prepared by W arc melting in a protective Ar atmosphere. Two alloy series were prepared with the following compositions: Fe-15Al-10Ni-*x*Mo (at. pct) and Fe-10Al-3Ni-*x*Mo (at. pct). The value of x was varied between 0 and 5 at. pct. The volume fractions (f_v) were determined to be 36 ± 0.4 pct and 6 ± 0.1 pct, respectively, by using surface analysis of two stage replicas. The procedure outlined by Hilliard and Cahn[18] was followed. Thin foil TEM analysis was also used to evaluate f_v. The foil thickness was estimated by the convergent beam technique[19] and the number of particles/cm^3, N_v, was determined by following Hilliard's varying thickness method.[20] The values obtained for f_v by the two different techniques differ by only 5 pct, which is within the expected experimental error of both techniques.

A study of the variation of lattice parameter misfit as a function of aging time and particle size was performed using an additional series of alloys which was prepared by the Inland Steel Company Research Laboratory. The nominal compositions and f_v's of these alloys are the following:

Alloy B, Fe-10Al-3Ni-1.5Mo (at. pct), $f_v = 7 \pm 0.5$ pct

Alloy C, Fe-10Al-3Ni-2.5Mo (at. pct), $f_v = 7 \pm 0.5$ pct

All alloys were solution treated at 1373 K for 1.5 hours. The alloys with low f_v were then quenched in iced water. The alloys with high f_v were quenched in oil at room temperature to avoid cracking. Slices were then obtained from the experimental samples and aged in vacuum at 973 K for times ranging from 1 to 400 hours.

Specimens for transmission electron microscopy (TEM) were prepared by electrolytically thinning in a twin jet apparatus with a solution of 22 vol pct nitric acid in methanol at 223 K. A voltage of 25 V corresponding to a current density of 0.8 A/cm^2 was used. Electron microscopy was performed in a 200 kV Hitachi H-700H analytical electron microscope.

The measurements of lattice parameter were carried out in an 11.4 cm diameter Debye-Scherer camera with Fe-filtered Co radiation. The powder samples were obtained by filing the solution treated bulk samples. The filings were sieved to −200 mesh before the aging treatments which were performed at 973 K in a vacuum of 10^{-6} torr. All specimens were furnace cooled to prevent the development of residual stresses. This procedure produced sharp diffraction lines and allowed the detection of weak superlattice reflections. A capillary of 0.2 mm in diameter was used to hold the sample powder together with Si powder as a calibration standard. The data were analyzed in two forms, by extrapolating to a value of lattice parameter corresponding to $\sin^2 \theta = 1$ (θ being the angle of diffraction) and by using the Nelson-Riley relationship. Results obtained by the two methods differed only in the fourth decimal place. The values reported here correspond to those calculated by extrapolation to $\sin^2 \theta = 1$.

III. RESULTS AND DISCUSSION

A. *Effect of Lattice Parameter Mismatch on Ostwald Ripening of NiAl Type Precipitates*

Figure 1 shows the X-ray measurements of δ, the room temperature lattice parameter misfit between matrix and precipitate, as a function of Mo content in the two alloy series Fe-10Al-3Ni-xMo ($f_v = 6 \pm 0.1$ pct) and Fe-15Al-10Ni-xMo ($f_v = 36 \pm 0.4$ pct). Samples in the first series were aged at 973 K for 10 hours; those in the second series for 25 hours. The misfit parameter δ is defined as $(a_0^{\beta'} - a_0^{\alpha})/a_0^{\alpha}$, where $a_0^{\beta'}$ is the lattice parameter of the precipitate and a_0^{α} that of the matrix. Note that the misfit values in Figure 1 pertain to particles embedded in the matrix; *i.e.*, these are constrained values of δ. At low Mo contents the value of a_0^{α} increases as Mo is added, an observation that suggests that Mo partitions preferentially to the matrix. In alloys having more than 1 at. pct Mo, Mo causes an expansion in the lattice of the precipitates and thus an increase in the value of δ. For the aging conditions listed above, the lattice disregistry is extremely low when the Mo content is 2.5 at. pct in the low f_v alloys and 1 at. pct in the high f_v material. In high volume fraction alloys with more than 2 at. pct Mo, a new Mo-rich phase appears, presumably the hexagonal ε phase, which is incoherent with the matrix. From this point on in the investigation only alloys without ε phase were studied.

The Ostwald ripening kinetics of β' particles in Fe-15Al-10Ni-(0, 1, 2) Mo alloys and Fe-9.7Al-3Ni-(0, 2.5, 4) Mo alloys at 973 K are shown in Figure 2. The values of the

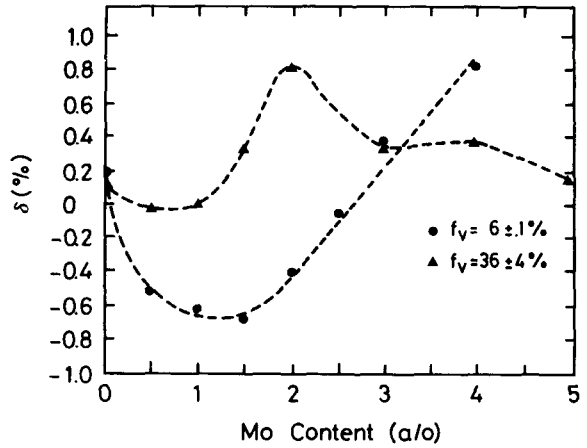

Fig. 1—Lattice parameter mismatch δ as a function of Mo content in Fe-10Al-3Ni-xMo (f_v = 6 ± 0.1 pct) and Fe-15Al-10Ni-xMo (f_v = 36 ± 0.4 pct) alloys. Alloys with f_v = 6 ± 0.1 pct were aged for 10 h and those with f_v = 36 ± 0.4 pct for 25 h, all at 973 K.

coarsening rate constants K for the alloys under study as obtained from the slopes of the lines in Figure 2[6–9] are given in Table I along with the corresponding initial values of δ. The interfacial energies have been calculated from the data in Table I with the assumption of coarsening according to the LSW theory.[6,7] The results were published in Reference 11. These calculated values are in the range expected for a coherent-coplanar precipitate-matrix interface.

As shown in Table I, the differences in the values of K corresponding to different Mo contents in alloys with high volume fraction (36 ± 0.4 pct), are comparatively smaller than in the case of the alloys with lower volume fraction

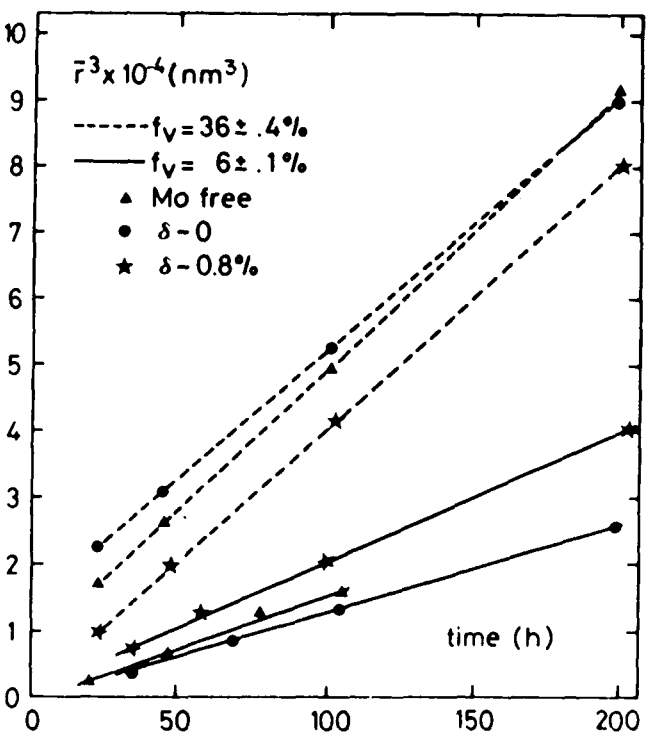

Fig. 2—Coarsening behavior of β' in Fe-Ni-Al-Mo alloys as a function of volume fraction f_v and lattice misfit δ measured on samples with shortest aging time. $\bar{r}$ indicates mean particle radius and is measured in nm.

(6 ± 0.1 pct). Nevertheless, the behavior is similar in both cases. The lowest initial δ gives rise to the slowest coarsening rate. Statistical analysis of the errors introduced during sampling and measurement of particle size yields the results given in the last column of Table I. The error introduced during sampling was evaluated according to standard techniques.[20] Analysis shows that measurement of 600 particles will introduce an error of approximately 0.5 pct in the determination of average particle size. Therefore the statistical error in the evaluation of K is never greater than 2 pct as may be seen from Table I.

B. *Particle Morphology*

The particle morphology of the alloys with low volume fraction (6 ± 0.1 pct) has been already described in References 5 and 11.

The β' particles in the high volume fraction Mo-free alloy were observed to undergo morphological changes during high temperature aging. Figure 3 shows the TEM images of β' precipitates in the Fe-10Ni-15Al alloys (f_v = 36 ± 0.4 pct) after different aging treatments at 973 K. At short aging times many particles with irregular shapes are found (Figure 3(a)). This may be attributed to coalescence of closely spaced particles. As suggested by Gu *et al.*[21] "encounters" between precipitates will produce an aspect ratio markedly different from one. Figure 4 shows a cumulative distribution of aspect ratios of particles in the Mo-free alloy after 26 hours of aging. More than 75 pct of the particles show an aspect ratio lower than 0.8. This suggests that the number of encounters may be of significance in this alloy when the particles are in close proximity. As the aging time is increased three different β' morphologies are observed: spherical, cuboidal, and parallelepiped rectangular. The particular shape depends on particle size (Figures 3(b) and (c)). Particles under 50 nm appear as spheres or cubes with rounded edges. Larger particles become cuboidal or rectangular parallelepipeds with faces aligned along ⟨100⟩ directions. A rectangular shape may indicate an encounter event in the past.

In contrast, precipitate particles in the alloys containing molybdenum remain spherical. Evidence of coalescence (*i.e.*, elongated or irregular shapes) is less frequently observed (see Figures 5 and 6). Figure 5(b) shows the dark-field image of the precipitates in the alloy Fe-15Al-10Ni-1Mo after 100 hours at 973 K. The spherical morphology is preserved for aging times as long as 800 hours at 973 K. This persistence of the spherical shape could be interpreted as a consequence of the reduction in lattice disregistry between

Table I. Volumetric Coarsening Rate K and Lattice Mismatch δ

Alloy	Volume Fraction (Pct)	δ (Pct)	K(nm^3/h)
Fe-15Al-10Ni	36 ± 0.4	+0.10*	397 ± 8
Fe-15Al-10Ni-1Mo	36 ± 0.4	+0.03*	377 ± 7.5
Fe-15Al-10Ni-2Mo	36 ± 0.4	+0.80*	401 ± 8
Fe-10Al-3Ni	6 ± 0.1	+0.21†	141 ± 3.5
Fe-10Al-3Ni-2.5Mo	6 ± 0.1	−0.06†	126 ± 3.4
Fe-10Al-3Ni-4Mo	6 ± 0.1	+0.80†	160 ± 4

*Aged 25 hours at 973 K
†Aged 10 hours at 973 K

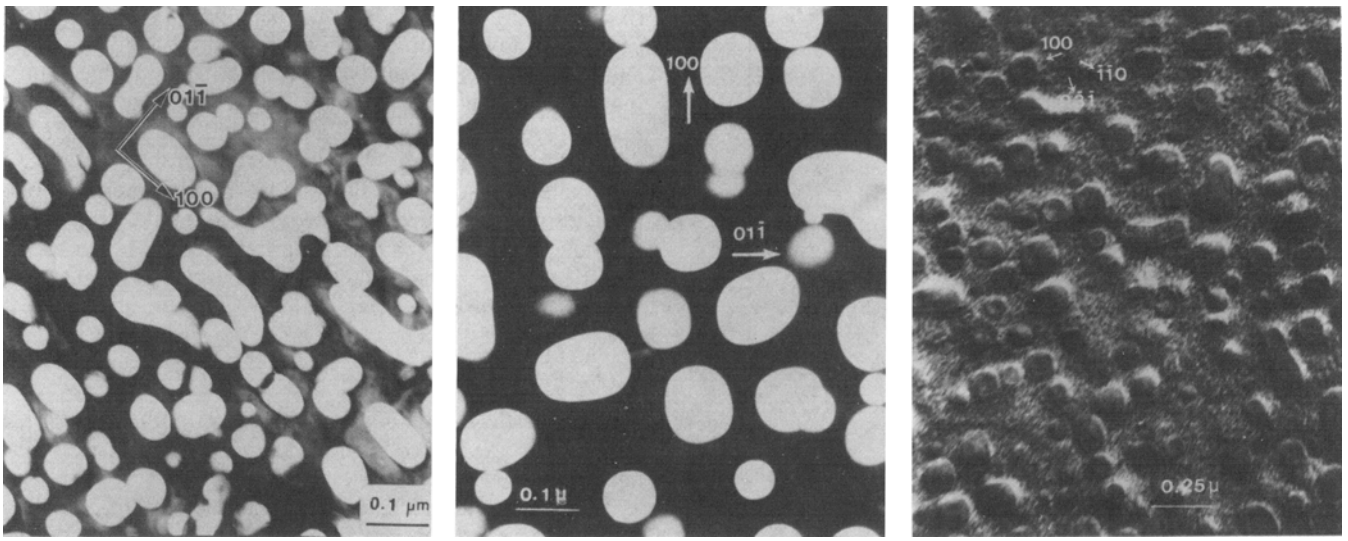

(a) (b) (c)

Fig. 3 — Morphology of NiAl type particles in Fe-15Al-10Ni alloy after different aging times at 973 K: (*a*) 100 h, (*b*) 200 h, (*c*) 200 h taken in two beam condition to show strain contrast.

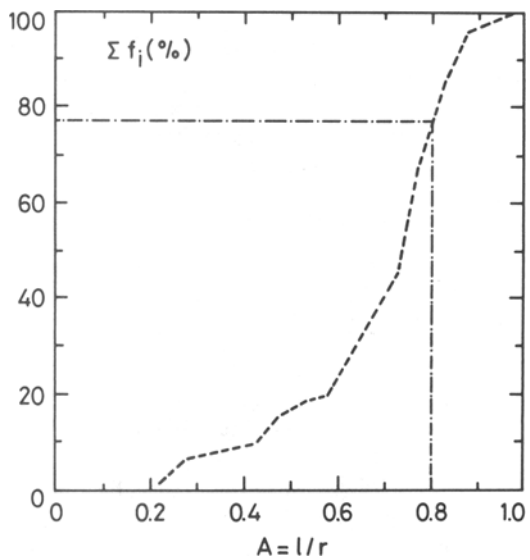

Fig. 4 — Cumulative distribution Σf_i of the aspect ratio $A(r/l)$ of precipitates in Fe-10Ni-15Al after 26 h at 973 K. r represents the particle radius and l its length.

matrix and precipitate in the alloy containing 1 at. pct Mo. However, the same morphology is found in the other Mo-containing alloys under study regardless of the lattice misfit between matrix and precipitate. The lattice misfits measured in this work ranged from 0 to 0.8 pct.

It is commonly accepted, following Ardell *et al.*,[22] that particle morphology is controlled by δ, but the present results suggest that δ is not the only parameter involved in the control of the morphology of the second phase particles in Fe-Ni-Al-Mo alloys. It is suggested that the addition of Mo may directly affect the interface composition as well as the global composition of the particles. Fine *et al.*[23] have already shown that solute segregation to the particle-matrix interface may reduce the interfacial energy σ. Their treatment is based on classical thermodynamics and is strictly valid only for fluid systems. The analysis put forward by Cahn and Larché[15] on the thermodynamics of stressed solids may be used to complement the treatment by Fine *et al.* According to Cahn and Larché,[15] in the case of small solid particles embedded in a solid matrix, three interface quantities should be considered, namely, the ordinary interfacial free energy σ° (related to the work of creating a surface) and two surface stresses: f (related to the work of straining the interface by straining both crystals) and g (related to the work of straining one crystal alone). Thus a new function σ must be defined. In the case of a spherical coherent particle, the stored strain energy and the surface free energy, which have an important role in the control of morphology, are shown to be functions of σ°, f, the particle size r, and the unconstrained lattice misfit δ_u (Eqs. [16] and [17] in Reference 15). Therefore, the present results suggest that addition of Mo markedly affects the value of the surface stress f and/or the interfacial free energy σ°, since different lattice misfits have been measured and no change in particle morphology is observed.

Segregation of Mo to the interface may reduce the surface strain on the basis of the Lechatelier principle. Cahn and Larché[15] have also shown that when elastic equilibrium is assumed, σ in a spherical particle has a radius dependence due to the strain produced by the interface stress and that compositional variations in the vicinity of the interface are possible on the basis of a criterion of minimum total free energy. Therefore the present results may be explained as the effect of segregation of Mo to the particle-matrix interface. Changes in the global composition and lattice parameter of the particles may be expected as the particle size increases, that is, with increased aging time. These variations in composition and lattice parameter have not yet been experimentally studied in the high f_v alloys. However, the change in lattice parameters observed in the Fe-Ni-Al-Mo alloys with a precipitate volume fraction of 7 ± 0.5 pct, as reported below, are interpreted in terms of a composition change.

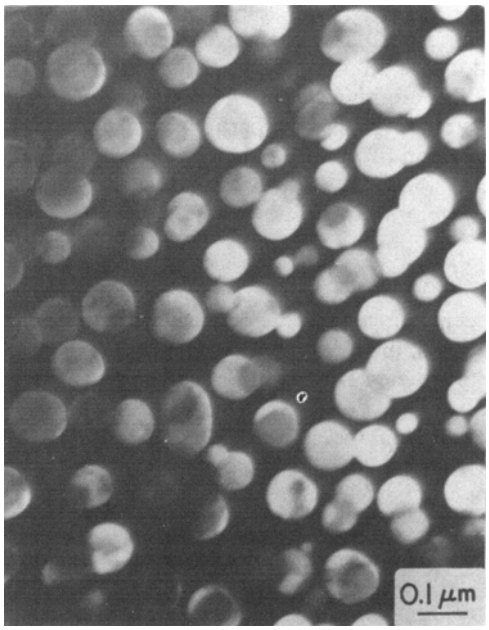

(*a*)

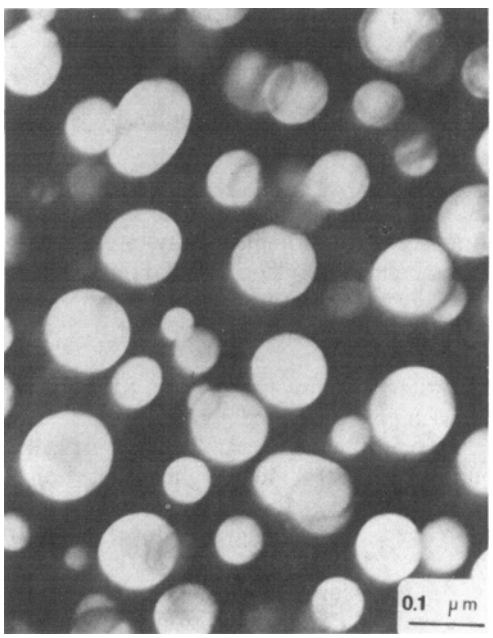

(*b*)

Fig. 5—Morphology of β' particles in Fe-15Al-10Ni-1Mo alloy aged at 973 K: (*a*) 50 h, (*b*) 100 h.

The TEM-images of the NiAl type particles in alloys with higher Mo content show regions of different contrast. The variability in contrast is especially noticeable after short aging times. Figure 6 illustrates the effect as observed in the Fe-15Al-10Ni-2Mo alloy aged 25 hours at 973 K. As discussed by Gu *et al.*[21] for the case of Al-base alloys, the contrast variation may be due to a difference either in composition or in ordering. The contrast variations in the alloy containing 2 at. pct Mo vanish after longer aging treatments. Nevertheless, contrast variations still may be observed in the particles of alloys with higher Mo contents after aging treatments as long as 200 hours at 973 K. If it is assumed that the differences in contrast arise only from compositional variation it is possible to determine a composition for the central region by calculating the structure factor F of the superlattice reflection used to image the particles. Identifying the lack of dark-field image with the condition $F(100) = 0$ yields a composition for the central region of the β' particles of Ni $(Al_{0.6}Mo_{0.4})$.

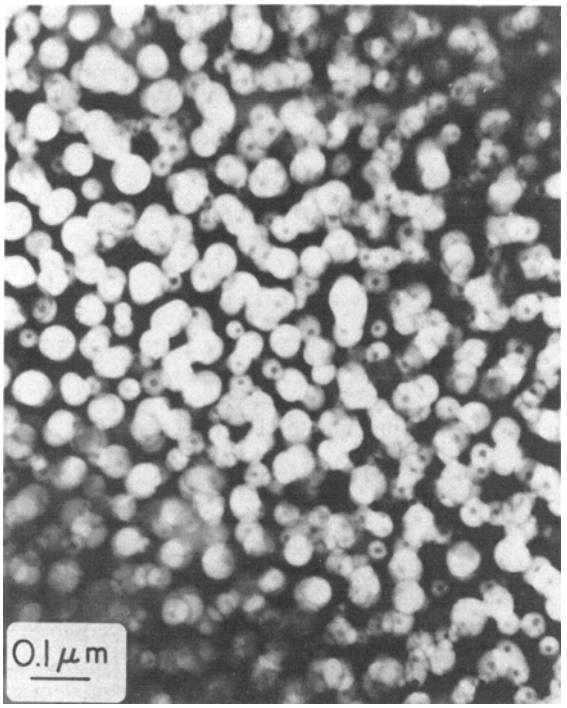

Fig. 6—Superlattice dark-field image of β' particles in Fe-15Al-10Ni-2Mo alloy after 25 h at 973 K. The central region of the particles is out of contrast because of a variation in composition or ordering.

C. *Effect of Volume Fraction of Precipitate on the Coarsening Kinetics of NiAl Type Particles*

As shown in Reference 11, an indication of the effect of volume fraction of precipitate on the Ostwald ripening of β' may be obtained from the data in Table I. Alloys with similar lattice misfit may be used to compare the experimental to the theoretically predicted results. Table II shows the ratio $K(36)/K(6)$ of the coarsening rate constants in two alloys with different values of f_v but with the same lattice misfit. $K(f_v)$ represents the experimental coarsening rate constant measured in the alloy with a volume fraction f_v. The ratios are evaluated for $\delta = 0$, $\delta = 0.8$ pct, and for the Mo-free alloys ($\delta = 0.1$ to 0.2 pct). The results obtained for the alloys with nearly zero mismatch are especially significant since these alloys are the closest approximation in a solid system to the current theoretical models which neglect the effect of elastic strain energy and therefore misfit strains. Table II also lists the ratio of coarsening rate constants predicted by the models for volume diffusion controlled coarsening proposed by Davies, Nash, and Stevens (DNS),[25] Brailsford and Wynblatt (BW),[8] and Voorhees and Glicksman (VG).[9]

The data in Table II clearly show that the Ostwald ripening process of these NiAl type particles is affected by the

Table II. Effect of Particle Volume Fraction on Coarsening Rate Constants

Model/δ (Pct)	$K(36)/K(6)$	$K'(36)/K'(6)$	$D(36)/D(6)$*
DNS[25]	1.35		
VG[9]	2.05		
BW[8]	2.07		
$\delta = 0$	2.99	2.55	1.24
$\delta = 0.8$	2.51	2.14	1.04
$\delta = 0.1$ to 0.2 (Mo-free)	2.82	2.41	1.16

*Calculated with $K(36)/K(6)$ from BW[8] and VG[9] models.

volume fraction of precipitate. The experimental values are always higher than the theoretical predictions, the difference ranging from 22 to 46 pct; the agreement is best for the BW and VG models. The disagreement may be related partly to changes in equilibrium solubility C_0 of NiAl in the matrix or diffusivity D of the controlling species (assumed to be Ni, as discussed in Reference 5) with volume fraction. The extent of the change in C_0 with increased f_v may be obtained by analyzing the Al-Fe-Ni ternary diagram.[2] It is assumed that the addition of the small amounts of Mo present in the alloys does not substantially alter the phase diagram. In this manner C_0 was estimated to be 0.0035 mol/cm^3 in the Fe-10Al-3Ni alloy and 0.0041 mol/cm^3 in the Fe-15Al-10Ni alloys. By dividing $K(f_v)$ by $C_0(f_v)$ the effect of changes in solubility can be eliminated. Table II lists values of the ratio of normalized coarsening rate constants $K'(36)/K'(6)$, where $K'(f_v) = K(f_v)/C_0(f_v)$. A somewhat better agreement between the experimental and the BW and VG theoretical values is now obtained but the experimental ratios are still higher than predicted. Table II also shows the necessary increase in D as f_v changes which would be needed to remove the remaining discrepancies between the measured values of coarsening rate ratios and those predicted by the BW and VG models. Little is known regarding the effect of solute concentration on diffusivity D. Further, the Mo contents of the precipitates and the degree of order for the two sets of alloys may not be the same. Thus the discrepancy between K' measured for the zero misfit alloy and the VG and BW theoretical values cannot be taken as disagreement with theory.

Some controversy exists regarding the effect of volume fraction on the coarsening kinetics. Chellman and Ardell[26] did not find any appreciable difference in the coarsening kinetics of precipitates in Ni-Al alloys with different volume fractions. Of course, if the coarsening kinetics is controlled by the interface reaction then no appreciable effect of f_v on the coarsening kinetics is predicted because the diffusion fields are very short ranged. However, the determination of particle size by Chellman and Ardell is highly questionable since coalescence of particles gave rise to rather complicated particle morphologies. On the contrary, the particle morphology in Fe-Ni-Al-Mo alloys was invariably spherical and little direct evidence of coalescence was observed in the alloys containing Mo.

Other researchers have found that the Ostwald ripening process is affected by f_v. The reported values disagree with the theoretical predictions. Table III summarizes a number of measurements found in the literature[27–30] of coarsening rate ratios at different precipitate volume fractions and compares these ratios with the predictions of the VG and BW models. The results of this investigation and the data in Table III agree in that for the most part the values of $K(f_v)/K(f'_v)$ are higher than theoretically expected. While these discrepancies may be partially explained on the basis of the variation of D and C_0 with solute content as already discussed, other factors such as chemical changes and the mismatch ratio need to be considered, too.

D. *Particle Size Distributions*

All the recent theoretical models which attempt to describe the bulk diffusion controlled Ostwald ripening kinetics of precipitates predict time independent particle size distributions (PSD's). Some of the PSD's obtained from measurements in the alloys Fe-10Al-3Ni-(2.5, 4)Mo are given in Figures 7 and 8, respectively. The PSD's corresponding to the Mo-free alloy have already been published.[5] One of them is reproduced in Figure 9 for the purpose of comparison. The predictions of the LSW theory and the BW model[8] are superimposed on the experimental histograms. The ordinate axes have been labeled "Probability density" and represent the quantity $\rho^2 h(\rho)$, where ρ is the normalized particle radius $r/\bar{r}$ and $h(\rho)$ is the size dependent function defined by Wagner.[7] Experimental values of $\rho^2 h(\rho)$ are calculated according to the relation:

$$\rho^2 h(\rho) = \frac{N_i(r, r + \Delta r)}{\sum N_i(r, r + \Delta r)} \frac{\bar{r}}{\Delta r}$$

where $N_i(r, r + \Delta r)$ represents the number of particles in a given class interval Δr. Analysis of the shape of the various PSD's is more easily accomplished by reference to the values of their moments or relations that directly involve them such as the skewness or kurtosis. Table IV shows the statistical parameters calculated from the experimental and theoretical distributions.

The quantitative analysis of the PSD's in Figures 7 through 9 is highly restricted by the sample size, which varied between 500 and 800 particles. A statistically reliable PSD requires the use of a much higher number of particles. This condition may be partially fulfilled by using all particle size measurements made on a given alloy after a sufficiently long aging time. Two assumptions are implicit in such a treatment: (1) coarsening is the predominant mechanism, and (2) a universal PSD exists during this regime. Measurements of microhardness and volume fraction of precipitate described elsewhere[5] suggest that after 10 hours at 973 K coarsening is indeed the predominant phenomenon. In addition, Venzl[31] has performed numerical calculations to investigate the time dependence of an assumed initial PSD. It was concluded that a unique distribution shape is obtained for a large number of starting conditions. Figure 10 shows the global PSD's obtained in the alloys Fe-10Al-3Ni-(0, 2.5, 4)Mo. Only particles measured in samples aged for 25 hours or longer are considered. The statistical parameters of these PSD's are also shown in Table IV. The agreement of the global PSD's with the theories is best for the Mo containing alloys where the skewness values have the same sign as the theoretical curves.

Figure 11 shows the PSD's obtained for the alloy Fe-15Al-10Ni-1Mo after 200 hours of aging at 973 K. This alloy has very small misfit. Approximately 1500 particles

Table III. Effect of Volume Fraction on the Coarsening Rate of Precipitates. Compilation of Published Empirical Data and Comparison with Predicted Values

System	$K(f_v)/K(f'_v)$ Theoretical VG[9]	$K(f_v)/K(f'_v)$ Theoretical BW[8]	$K(f_v)/K(f'_v)$ Experimental	f_v	f'_v	Ref.
60Cu-40Co	1.26	1.13	1.34	0.42	0.34	27
50Cu-50Co	1.69	1.30	1.83	0.55	0.34	27
Cu-1.3Co	1.30	1.36	1.30	0.011	0.004	28
Cu-2Co	1.56	1.65	1.39	0.019	0.004	28
Cu-3.2Co	1.95	2.05	3.20	0.033	0.004	28
Fe-Cu	1.08	1.05	1.28	0.55	0.51	29
Fe-Cu	1.35	2.71	1.96	0.67	0.51	29
Fe-Cu	1.96	1.33	3.83	0.84	0.51	29
Fe-Cu	2.02	1.35	4.35	0.86	0.51	29
Cu-Ag	1.36	1.12	1.61	0.75	0.59	29
Cu-Ag	1.91	1.25	2.39	0.90	0.59	29
MgO-Fe	1.20	1.43	1.43	0.029	0.006	30
MgO-Fe	1.27	1.55	1.77	0.034	0.006	30
MgO-Fe	1.13	1.32	1.50	0.017	0.0065	30
MgO-Fe	1.27	1.43	1.80	0.030	0.0065	30

were measured in the construction of the histogram. More details about the distribution are given in Reference 11. The predictions of two theoretical models are superimposed on the data. Both models predict PSD's which are very similar to the one experimentally found. The VG model[9] shows a slightly better agreement, although this may be fortuitous since these two models are strictly valid only in the case of a fluid phase.

E. *Variation of Lattice Parameter Misfit with Particle Size*

The curves of Figures 12(a) and (b) show the variation of lattice parameter (measured at room temperature) of the precipitate and matrix phases as a function of aging time in alloys B and C. It can be seen that at relatively short aging times the lattice parameter of the precipitate $a_o^{\beta'}$ changes very rapidly. As aging progresses $a_o^{\beta'}$ varies more slowly and becomes approximately constant. The lattice parameter of the matrix decreases with aging, but the overall change is less than that of the β' particles. Figure 12(c) shows the variation of the lattice misfit with aging time. The misfit approaches a stable value after some time of aging. The variation of lattice parameters may be related to average particle sizes during coarsening from the $\bar{r}^3$ *vs* t data.

The a_o's of the precipitate and matrix are nearly the same for small particles and diverge as the particles grow. Of course, the a_o's should be considered at the aging temperature rather than at room temperature, but the coefficient of expansion difference may give only a second order effect.

The observed variation of lattice parameters during the coarsening process may be related to the minimization of the sum of the strain energy produced by the lattice disregistry between matrix and precipitate and the interfacial energy. The strain energy increases with r^3 while the surface energy increases as r^2. Thus it is to be expected that small particles are coherent while at least a partial loss of coherency occurs as the particles grow. Reduction of strain energy may be achieved *via* compositional changes in the matrix or precipitates and/or by dislocation generation at the particle-matrix interface. The NiAl precipitates in the alloys under study were perfectly coherent during the initial stages of coarsening as shown by electron microscopy (aging times between 10 and 200 hours). However, after long aging treatments, dislocations were observed. Figure 13 shows a weak beam image of the β' precipitates in alloy C after 450 hours at 973 K. Composition change may be proposed as a cause of the variation of δ with aging time for small particles but interface dislocations definitely are present when the particles become larger.

An estimate can be made regarding the particle size at which the loss of coherency begins. In this context, coherency loss means the generation of at least one dislocation at the particle-matrix interface. According to Brown and Ham,[32] originally coherent particles lose coherency with the matrix when $r > b/\delta$, where r is the particle radius and b is the burgers vector of the dislocation. A strong variation of $a_o^{\beta'}$ with aging time is observed up to 200 hours of aging at 973 K in alloy B and 100 hours in alloy C (Figure 12). Therefore, the values of δ corresponding to these aging conditions will be used in the evaluation of the radius at which coherency is lost. Coherency is expected to be lost when the particle size reaches 37 nm in alloy B and 27.5 nm in alloy C if b is identified with the normal glide dislocation b_{111}. On the other hand, if b_{112} (one of the possible partial dislocations) is used, the results are 29 and 21.5 nm in alloys B and C, respectively. Figures 12(a) and (b) indicate that both sets of calculated particle sizes for coherency loss agree reasonably well with the turnover in the $a_o^{\beta'}$ *vs* $\bar{r}$ curves. Since there is a distribution of particle sizes, coherency will be lost over a range of aging times. Thus it is difficult to determine precisely where coherency loss should occur in the curves of Figure 12.

The strong dependence of $a_o^{\beta'}$ on aging time at short times may be related to compositional changes in both matrix and precipitates. Specifically, diffusion of Mo from matrix to precipitate may create an increase in $a_o^{\beta'}$ since Mo has an atomic size larger than Fe, Ni, or Al. The relatively small change in a_o^{α} may be explained by considering the low

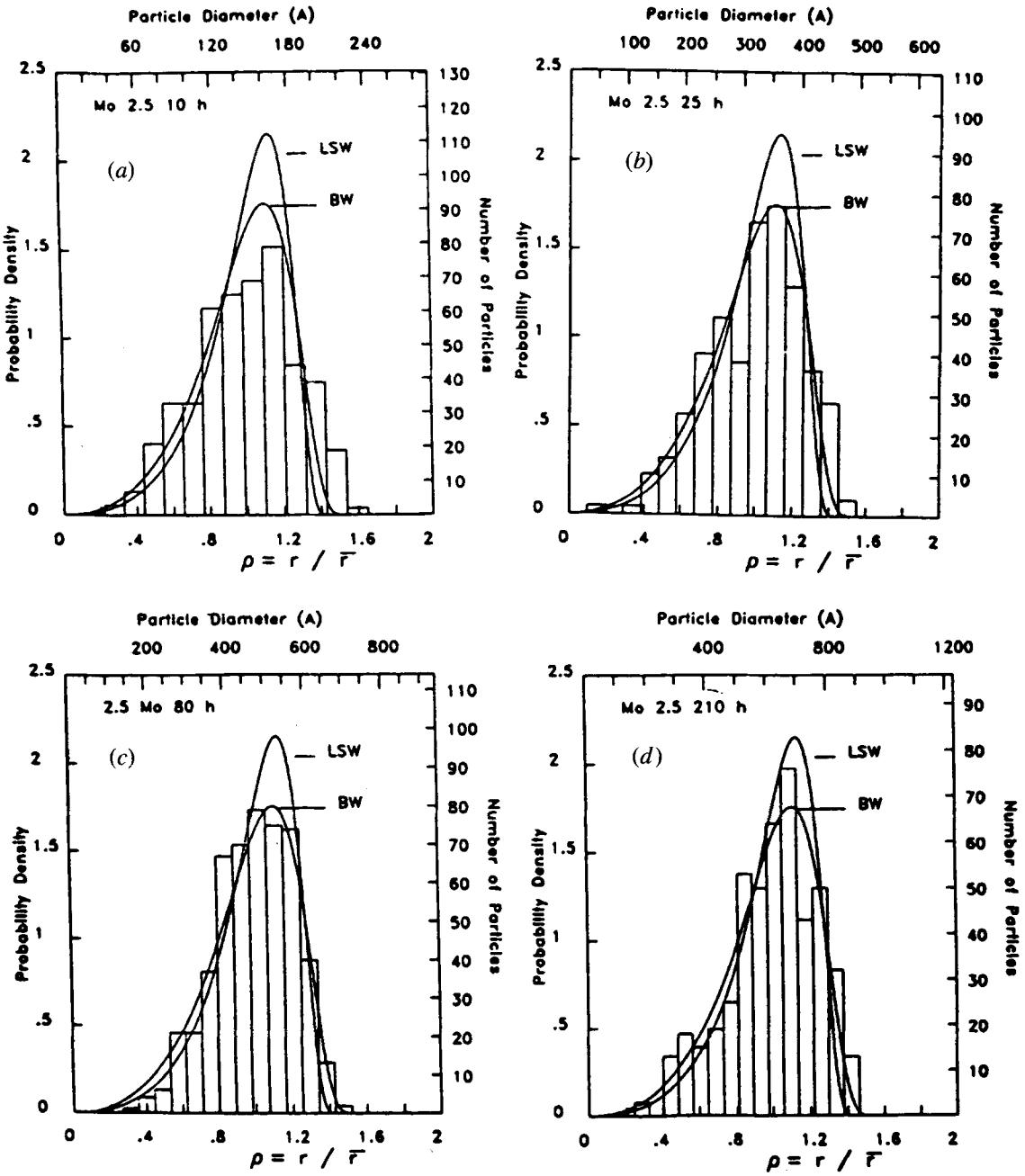

Fig. 7—Particle size distributions in Fe-10Al-3Ni-2.5Mo alloy aged at 973 K: (*a*) 10 h, (*b*) 25 h, (*c*) 80 h, (*d*) 210 h.

volume fraction of precipitate in the alloys under analysis. Thus, a small Mo depletion in the matrix would cause considerably larger variation in the lattice constant of the precipitate. In addition, it is likely that the compositions near the interface may adjust to reduce coherency strains. The effect of such changes on the measured values of a_o may be expected to decrease with increase of particle size since the near surface region will represent a progressively smaller fraction of the particle. The present observations are by no means isolated or unique. Theoretically, Johnson and Voorhees[13] have been able to predict enhancement of solute concentration around two misfitting particles and, although changes in concentration of the particles are not allowed in the theoretical treatment, the current results suggest that it may be a necessary consequence of the system's tendency toward equilibrium, as suggested by Cahn and Larché.[15] Gradients of composition around β' precipitates in Fe-20Cr-2Al-2Ni alloy were observed by Blavette *et al.*[33] using FIM.

Finally, it should be noted that the dependence of δ on aging time means that the coarsening curves of Figure 2 were taken under changing conditions of lattice misfit. The

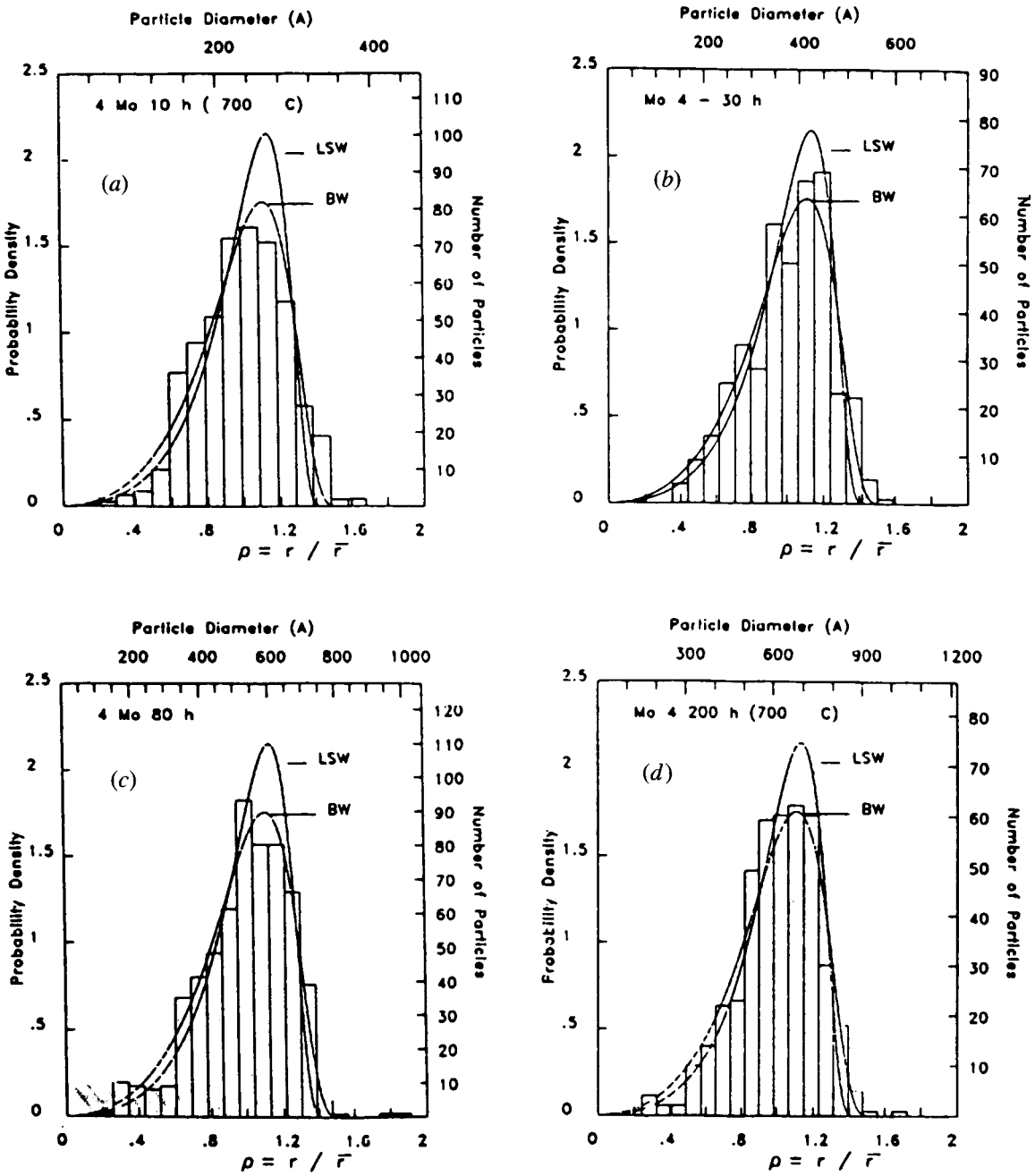

Fig. 8—Particle size distributions in Fe-10Al-3Ni-4Mo alloy aged at 973 K: (*a*) 10 h, (*b*) 30 h, (*c*) 80 h, (*d*) 200 h.

listed values of δ refer only to initial conditions and increase throughout aging. This effect would tend to produce an apparent value of K which is too high.

IV. CONCLUDING REMARKS

A study has been made on the effects of exposure to high temperature (973 K) on the ordered NiAl (β') particles in a series of Fe-Ni-Al alloys with and without the addition of Mo. Conclusions on this investigation are listed below:

The lattice parameter disregistry between matrix and precipitate is affected by Mo addition to Fe-Ni-Al alloys. In a series of alloys with similar precipitate volume fraction but various lattice mismatch parameters, the rate of precipitate coarsening during isothermal aging is slowest in the alloy with the lowest mismatch. This effect is more pronounced in alloys with low volume fraction ($f_v = 6 \pm 0.1$ pct).

The coarsening rate of the NiAl particles increases with increasing precipitate volume fraction. This enhancement in coarsening rate is greater than theoretically predicted, even after corrections are made for changes in the equilibrium solute concentration C_0.

The lattice parameter of the precipitated phase and of the matrix were found to be functions of aging time (and consequently of the average precipitate particle radius) in Fe-Ni-Al-Mo alloys with a volume fraction of 7 ± 0.5 pct. A change in the composition of the particles as well as ulti-

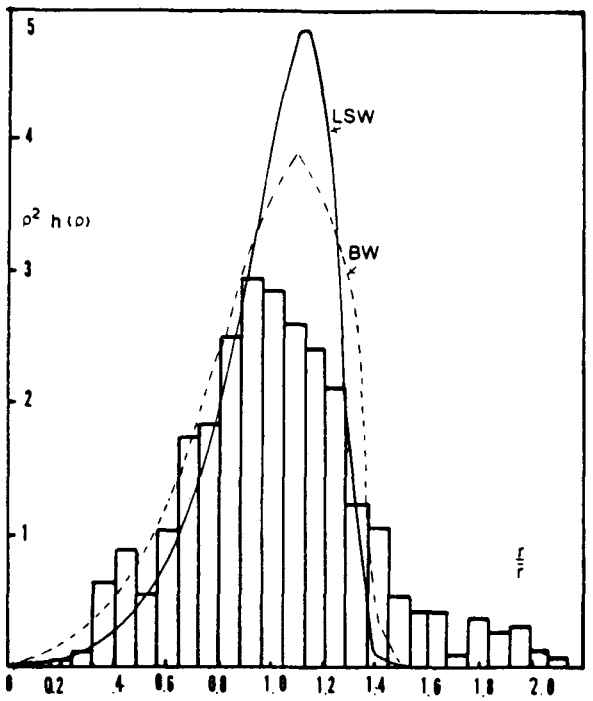

Fig. 9—Particle size distribution in Fe-10Al-3Ni alloy aged 100 h at 973 K.[5]

mately the loss of coherency upon continued aging may be responsible for these changes in the lattice constants.

In alloys with high volume fraction (f_v = 36 ± 0.4 pct) Mo addition impedes particle morphology changes and possibly coalescence of particles. Whereas the originally spherical small β' particles in the Mo free alloy become somewhat cubic or even resemble rectangular parallelepipeds after aging at 973 K, the β' particles in the alloys containing Mo continue to be spherical even after extended periods of aging. It is proposed that segregation of Mo to the particle-matrix interface and/or variation of the surface stress influence the particle morphology. Contrast effects in the particles show that the composition or ordering of the precipitates depends on aging time in alloys with higher Mo content.

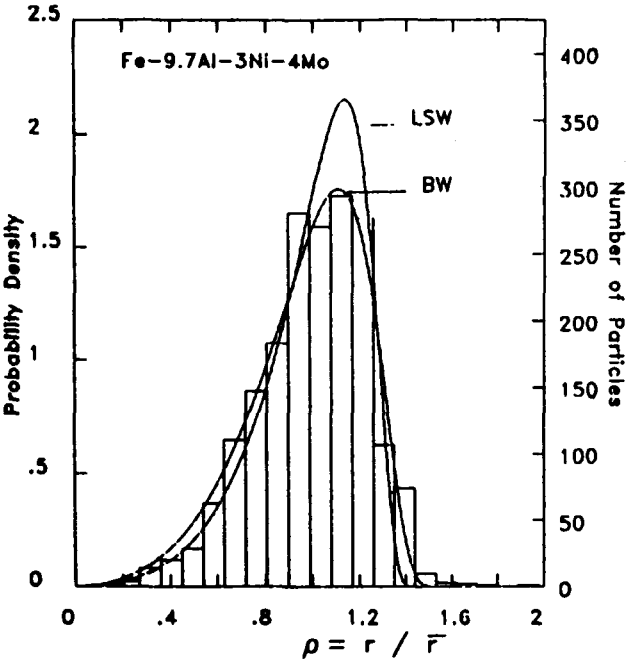

(*b*)

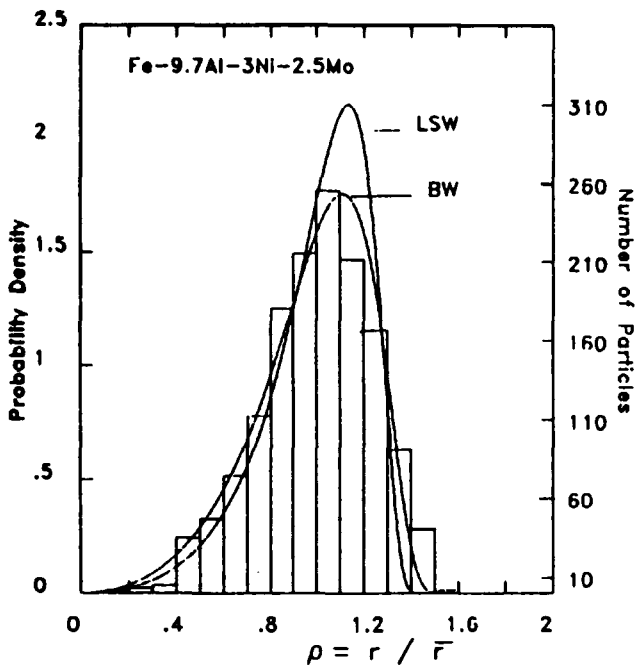

(*a*)

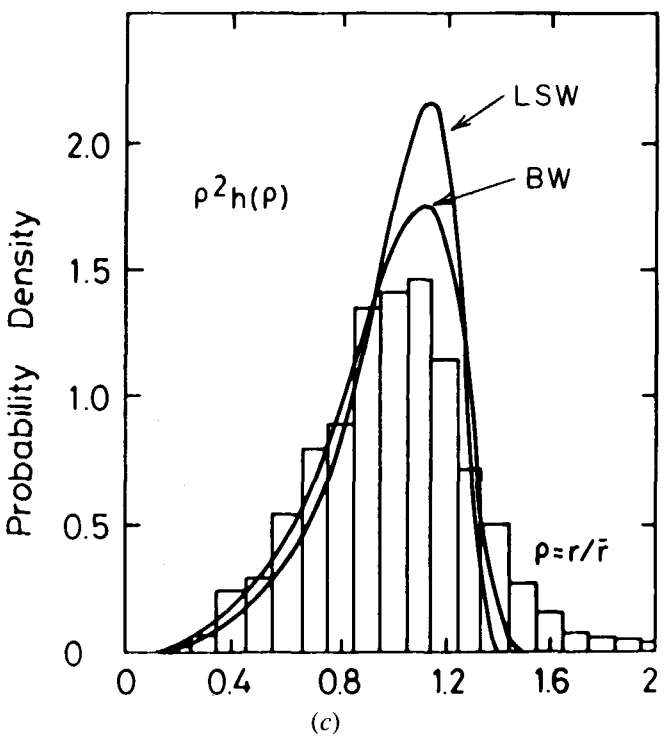

(*c*)

Fig. 10—Global particle size distributions, (*a*) Fe-10Al-3Ni-2.5Mo alloy, δ = 0 pct, (*b*) Fe-10Al-3Ni-4Mo alloy, δ = 0.8 pct, (*c*) Fe-10Ni-3Ni alloy, δ = 0.2 pct. Aging treatment of 25 h or longer at 973 K.

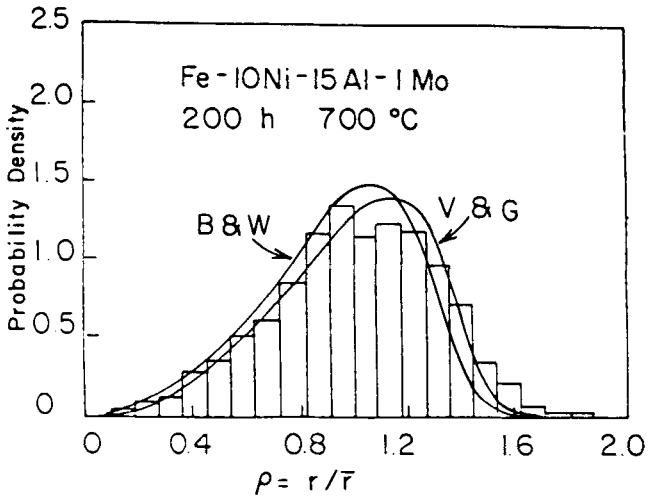

Fig. 11 — Particle size distribution in Fe-15Al-10Ni-1Mo alloy after aging 200 h at 973 K.[12] The theoretical predictions of the VG and BW models[8,9] are superimposed.

The size distribution of the β' particles have been measured in alloys subjected to aging. Good agreement is found between theory and experiment regarding the shape of the PSD's in the alloys with an $f_v = 36 \pm 0.4$ pct after 200 hours at 973 K. The PSD's obtained in the alloys with low volume fraction do not agree well with the predictions of the BW or VG model. The distributions are in general more symmetrical than predicted and do not show the predicted sharp cutoff in particle size on the high radius side. The global PSD's, involving all the particles measured for a given alloy, show better agreement with the theoretical models. However, they also are more symmetrical than predicted.

ACKNOWLEDGMENTS

One of the authors (HAC) wishes to acknowledge the financial support from the Government of Mexico through a Consejo Nacional de Ciencia y Tecnologia Fellowship. The authors express their appreciation to Inland Steel Com-

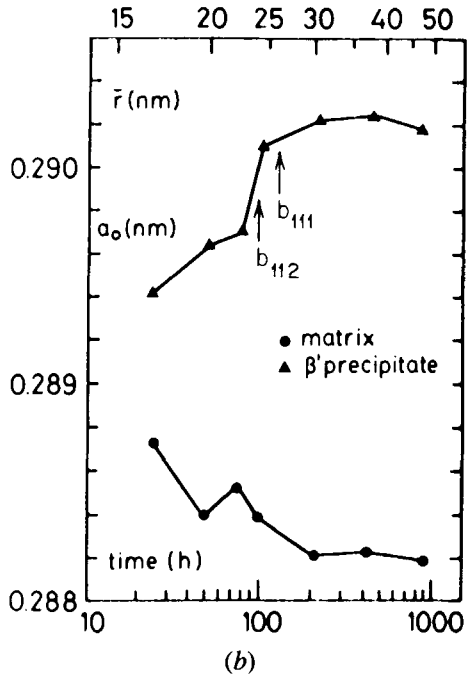

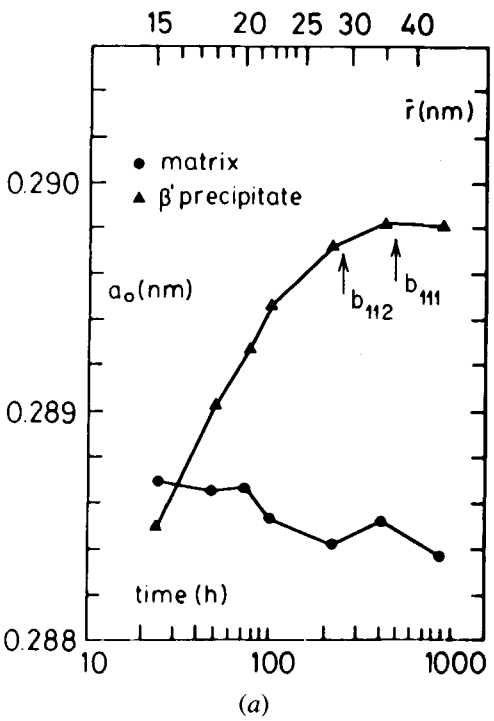

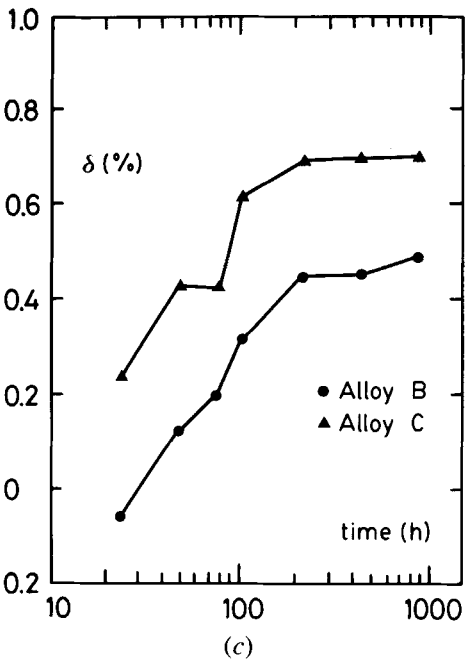

Fig. 12 — (*a*) Variation of lattice parameter a_o of matrix and precipitate as a function of particle size $\bar{r}$ and aging time in alloy B, (*b*) same as (a) for alloy C, (*c*) variation of lattice parameter mismatch δ with aging time at 973 K. Arrows indicate the particle radius at which coherency will be lost (see text).

Table IV. Parameters of Particle Size Distribution Functions in Fe-10Al-3Ni-xMo Alloys

Mo Content	Standard Deviation	Skewness	Kurtosis	Aging Time (h)	No. Particles in Distribution
0	0.29	0.004	2.68	5	674
0	0.23	− 0.18	2.95	23	734
0	0.28	− 0.25	2.65	50	688
0	0.35	0.51	3.50	100	589
Global	0.30	0.26	3.36		2011
2.5	0.27	− 0.21	2.77	10	475
2.5	0.25	− 0.38	2.63	25	455
2.5	0.21	− 0.61	3.46	80	510
2.5	0.24	− 0.51	3.42	210	474
Global	0.24	− 0.44	3.22		1440
4	0.24	− 0.21	2.77	10	472
4	0.23	− 0.38	2.63	25	408
4	0.25	− 0.61	3.46	80	588
4	0.22	− 0.51	3.42	200	422
Global	0.23	− 0.44	3.22		1418
BW[8]	0.24	− 0.68	3.13		
VG[9]	0.24	− 0.83	3.39		
DNS[25]	0.25	− 0.45	3.15		

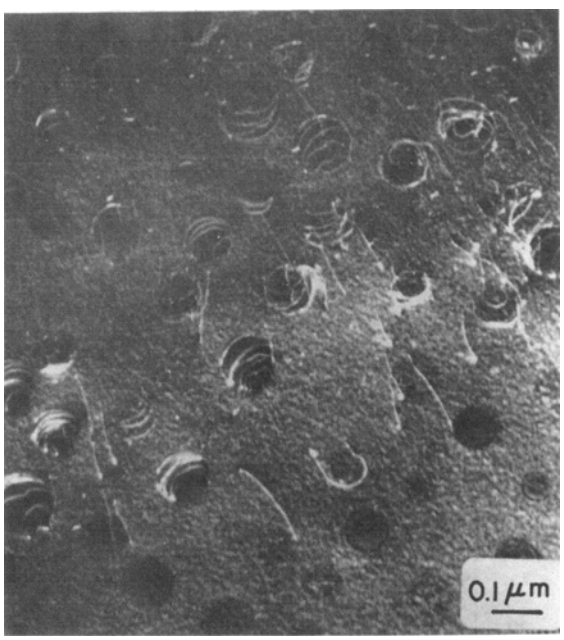

Fig. 13 — Weak beam image of microstructure of alloy C after 450 h at 973 K. Interface dislocations can be seen in large particles.

pany for supplying some of the alloys used in this study. This research was partially supported by the Materials Research Center of Northwestern University under NSF-MRL Grant DMR-8216972.

REFERENCES

1. W. B. Pearson: *Handbook of Lattice Spacing and Structure of Metals*, Pergamon Press, 1958, p. 347.
2. A. J. Bradley: *J. Iron & Steel Inst.*, 1951, vol. 168, pp. 233-44.
3. S. C. Kolesar: Ph.D. Thesis, Northwestern University, Evanston, IL, 1971.
4. M. E. Fine: *Metall. Trans. A*, 1975, vol. 6A, pp. 625-30.
5. H. Calderon and M. E. Fine: *Mat. Sci. Eng.*, 1984, vol. 63, pp. 197-208.
6. I. M. Lifshitz and V. V. Slyozov: *J. Phys. Chem. Sol.*, 1962, vol. 19, pp. 35-50.
7. C. Wagner: *Z. Electrochem.*, 1961, vol. 65, pp. 581-91.
8. A. D. Brailsford and P. Wynblatt: *Acta Metall.*, 1979, vol. 27, pp. 489-97.
9. P. W. Voorhees and M. E. Glicksman: *Chem. Phys. of Rapidly Solidified Materials*, B. L. Berkowitz and R. O. Scattergood, eds., TMS-AIME, Warrensdale, PA, 1983, p. 63.
10. J. A. Marqusee and J. Ross: *J. Chem. Phys.*, 1984, vol. 80, pp. 536-43.
11. H. A. Calderon, J. R. Weertman, and M. E. Fine: *Proc. of ICSMA 7*, Montreal, Pergamon Press, Oxford, 1985, vol. 1, pp. 737-42.
12. F. Larché and J. W. Cahn: *Acta Metall.*, 1973, vol. 21, pp. 1051-63.
13. W. C. Johnson and P. W. Voorhees: *Metall. Trans. A*, 1985, vol. 16A, pp. 337-47.
14. P. W. Voorhees and W. C. Johnson: *J. Chem. Phys.*, 1986, vol. 84, pp. 5108-21.
15. J. W. Cahn and F. Larché: *Acta Metall.*, 1982, vol. 30, pp. 51-56.
16. M. V. Nathal and L. J. Ebert: *Metall. Trans. A*, 1985, vol. 16A, pp. 1849-62.
17. A. Havalda: *Trans. ASM*, 1969, vol. 62, pp. 477-80.
18. J. E. Hilliard and J. W. Cahn: *Trans. ASM*, 1961, vol. 221, pp. 344-52.
19. P. M. Kelly, A. Jostsons, R. G. Blake, and J. G. Napier: *Phys. Stat. Sol.*, 1975, vol. A 31, pp. 771-80.
20. J. E. Hilliard: *Trans. ASM*, 1962, vol. 224, pp. 906-17.
21. B. P. Gu, G. L. Liedl, T. H. Sanders, Jr., and K. Welpmann: *Mat. Sci. Eng.*, 1985, vol. 76, pp. 147-57.
22. A. J. Ardell, R. B. Nicholson, and J. D. Eshelby: *Acta Metall.*, 1966, vol. 14, pp. 1295-1309.
23. M. E. Fine, Y. Chen, J. Conley, and J. Caputi: *Scripta Metall.*, 1986, vol. 20, pp. 743-44.
24. P. Schwander and H. Calderon: unpublished research, ETH-Zurich, 1987.
25. C. K. L. Davies, P. Nash, and R. N. Stevens: *Acta Metall.*, 1980, vol. 28, pp. 179-89.
26. D. J. Chellman and A. J. Ardell: *Acta Metall.*, 1974, vol. 22, pp. 577-88.
27. C. H. Kang and D. N. Yoon: *Metall. Trans. A*, 1981, vol. 12A, pp. 65-69.
28. J. D. Livingston: *Trans. AIME*, 1959, vol. 215, pp. 566-71.
29. R. Watanabe and Y. Masuda: *Mat. Sci. Res.*, 1974, vol. 10, pp. 389-98.
30. E. W. Kruse, III: Ph.S. Thesis, Northwestern University, Evanston, IL, 1970.
31. G. Venzl: *Ber. Bunsenges. Phys. Chem.*, 1983, vol. 87, pp. 318-24.
32. L. M. Brown and R. K. Ham: *Strengthening Methods in Crystals*, A. Kelly and R. B. Nicholson, eds., App. Sci. Ltd., London, 1971, p. 9.
33. D. Blavette, C. Martin, and G. Gallop: *Scripta Metall.*, 1982, vol. 16, pp. 59-64.